Supplementary Information

Theoretical designing of high-performance halogen anion batteries with MXene electrodes: influence of functional groups, metals, and anions

Jun Zhao[a], Ninggui Ma[a], Tairan Wang[a], Na Li[a], Yuhang Wang[a], Jun Fan[a, b*]

[a] Department of Materials Science and Engineering, City University of Hong Kong, Hong Kong, China;

[b] Center for Advanced Nuclear Safety and Sustainable Development, City University of Hong Kong, Hong Kong, China;
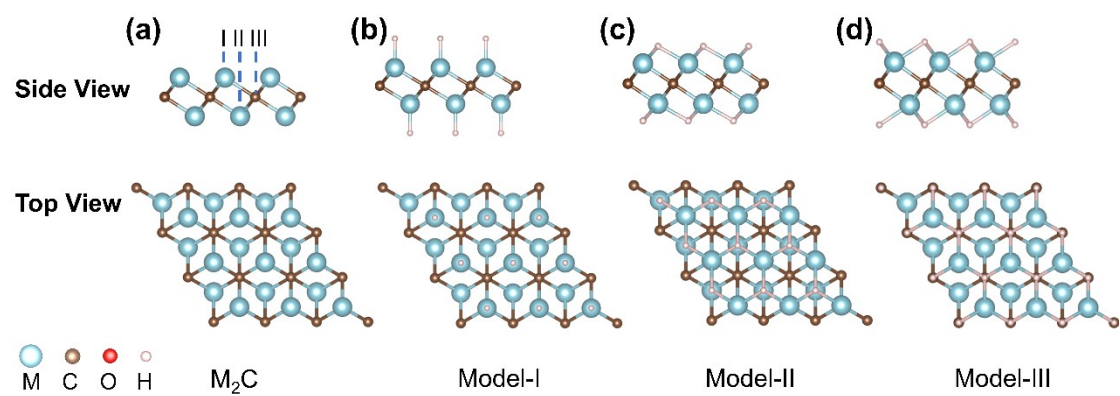
* Corresponding author. E-mail: junfan@cityu.edu.hk

Fig. S1 Side and top views of bare MXene (a), and three possible H-functionalized MXene models (b-d).
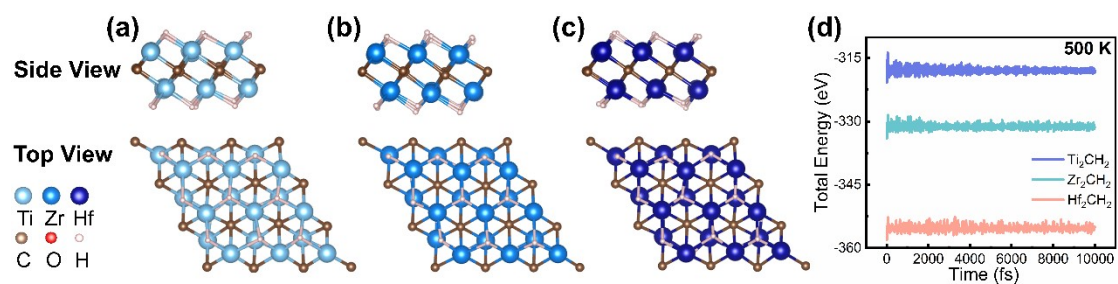
Fig. S2 AIMD simulation results of H-functionalized MXenes: structure of Ti_2CH_2 (a), Zr_2CH_2 (b), and Hf_2CH_2 (c) after 500 K, 10ps; variation curves in total energy of H-functionalized MXenes (d).
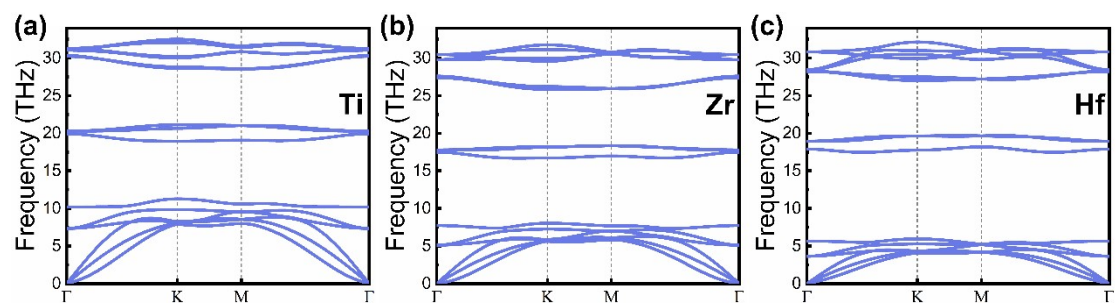

Fig. S3 Phonon spectrum of H-functionalized MXenes: Ti_2CH_2 (a), Zr_2CH_2 (b), Hf_2CH_2 (c).
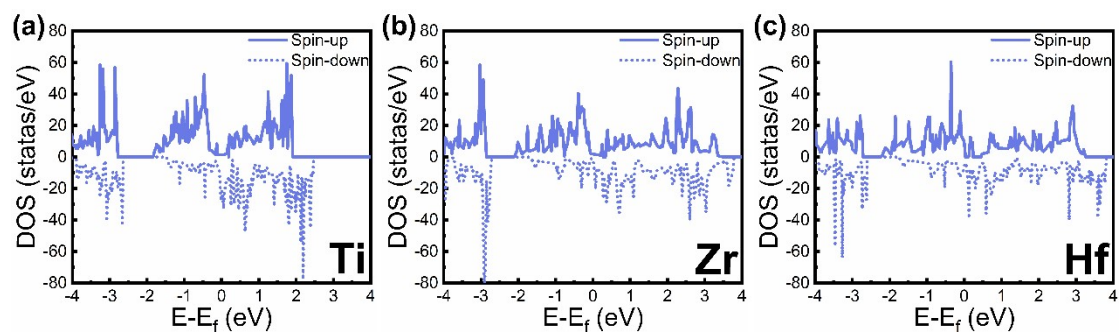
Fig. S4 DOS curves of all bare MXenes: Ti_2C (a), Zr_2C (b), Hf_2C (c). The Fermi energy level was set to 0 eV.
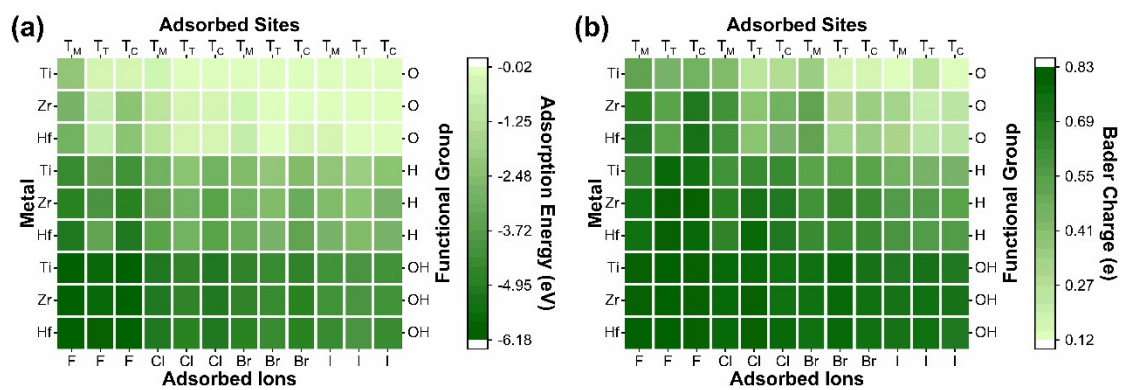
Fig. S5 Heat-maps of adsorption energy (a) and Bader charge (b) for all adsorbed sites on all functionalized MXenes.

Fig. S6 Differential charge density of Ti_2CO_2 (a), Ti_2CH_2 (b) and $Ti_2C(OH)_2$ (c); yellow region indicates charge accumulation, and blue region indicates charge loss; the value of the iso-surface was set to be 0.00025 e/$Å^3$. Total averaged potential (blue solid lines) along the axis perpendicular to the surfaces of Ti_2CO_2 (d), Ti_2CH_2 (e), and $Ti_2C(OH)_2$ (f). The vertical green lines indicate the position of the outmost surface atoms. The Symbol Φ represents the work function.
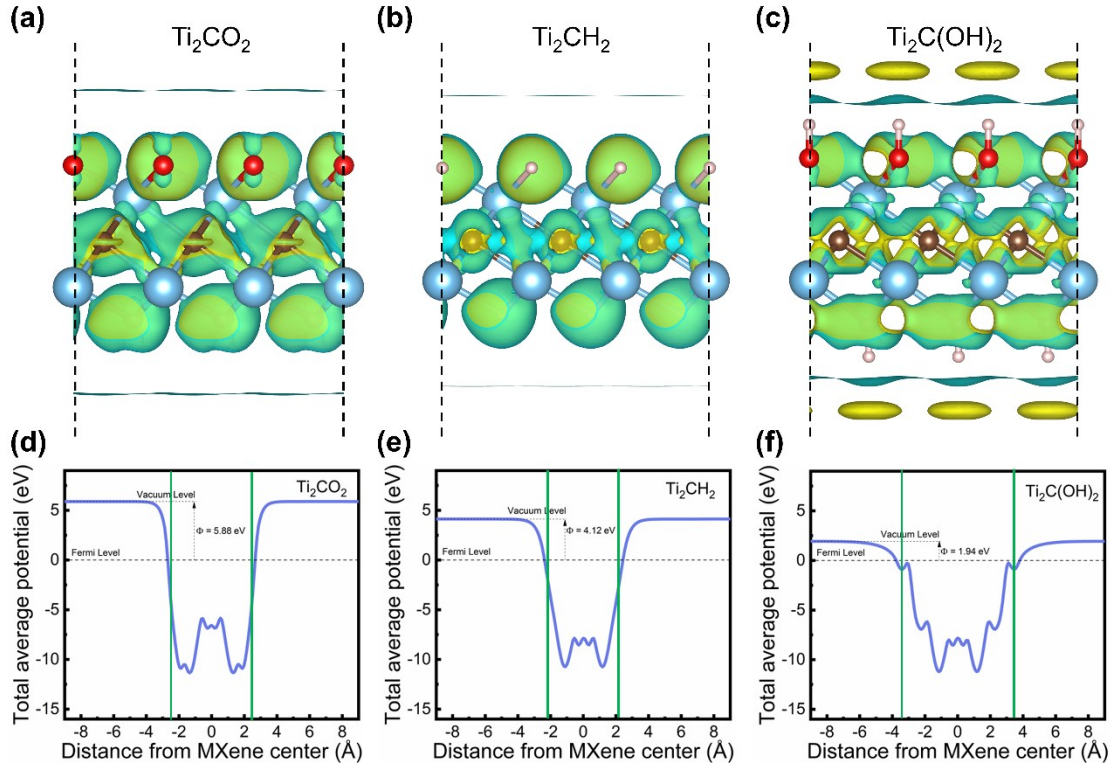
Fig. S7 Differential charge density of Zr_2CO_2 (a), Zr_2CH_2 (b) and $Zr_2C(OH)_2$ (c); yellow region indicates charge accumulation, and blue region indicates charge loss; the value of the iso-surface was set to be 0.00025 e/Å^3. Total averaged potential (blue solid lines) along the axis perpendicular to the surfaces of Zr_2CO_2 (d), Zr_2CH_2 (e), and $Zr_2C(OH)_2$ (f). The vertical green lines indicate the position of the outmost surface atoms. The Symbol Φ represents the work function.
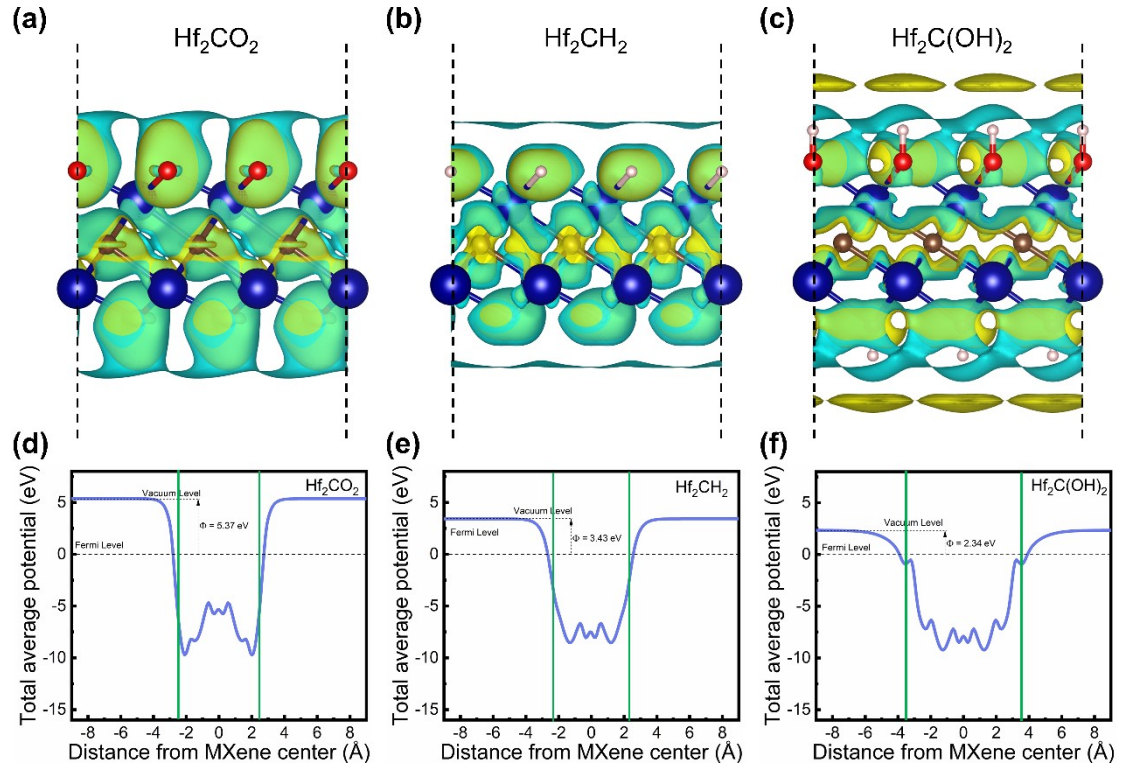
Fig. S8 Differential charge density of Hf_2CO_2 (a), Hf_2CH_2 (b) and $Hf_2C(OH)_2$ (c); yellow region indicates charge accumulation, and blue region indicates charge loss; the value of the iso-surface was set to be 0.00035 e/$Å^3$. Total averaged potential (blue solid lines) along the axis perpendicular to the surfaces of Hf_2CO_2 (d), Hf_2CH_2 (e), and $Hf_2C(OH)_2$ (f). The vertical green lines indicate the position of the outmost surface atoms. The Symbol Φ represents the work function.

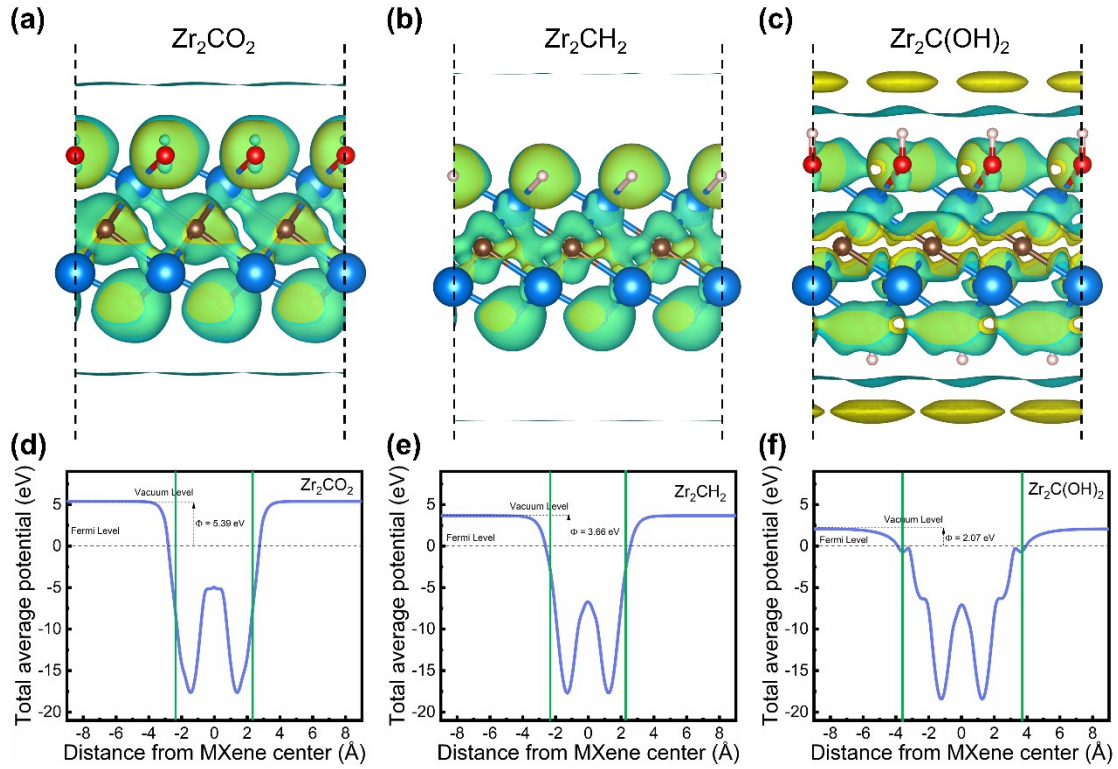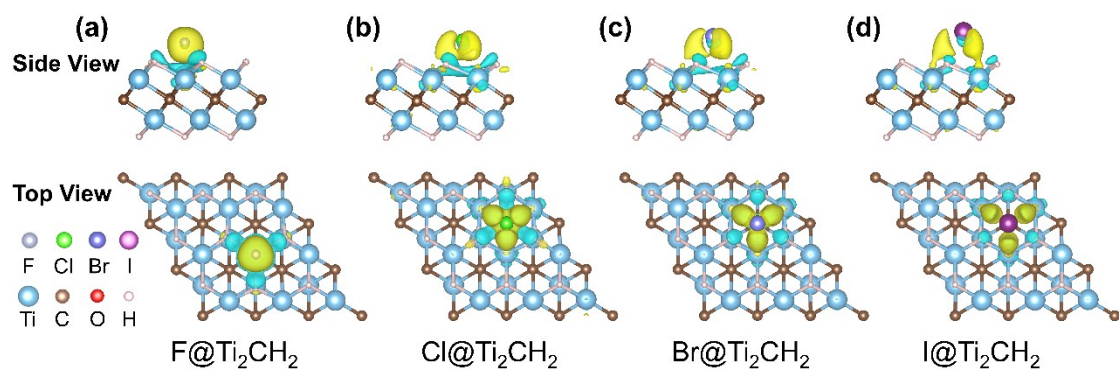**Fig. S9** Differential charge density of absorbed halogen ions on Ti_2CH_2 MXene; yellow region indicates charge accumulation, and blue region indicates charge loss. The value of the iso-surface was set to be 0.035 $e/Å^3$.
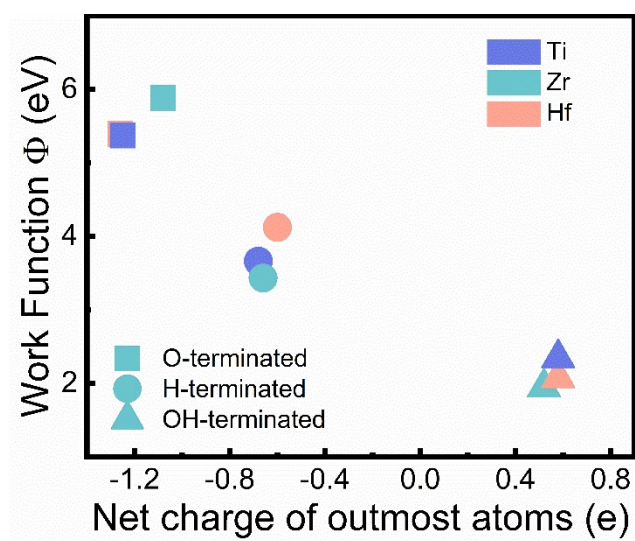
Fig. S10 The function between the work function and the net charge of the surface atoms. The positive net charge means losing electrons and the negative charge means gaining electrons.
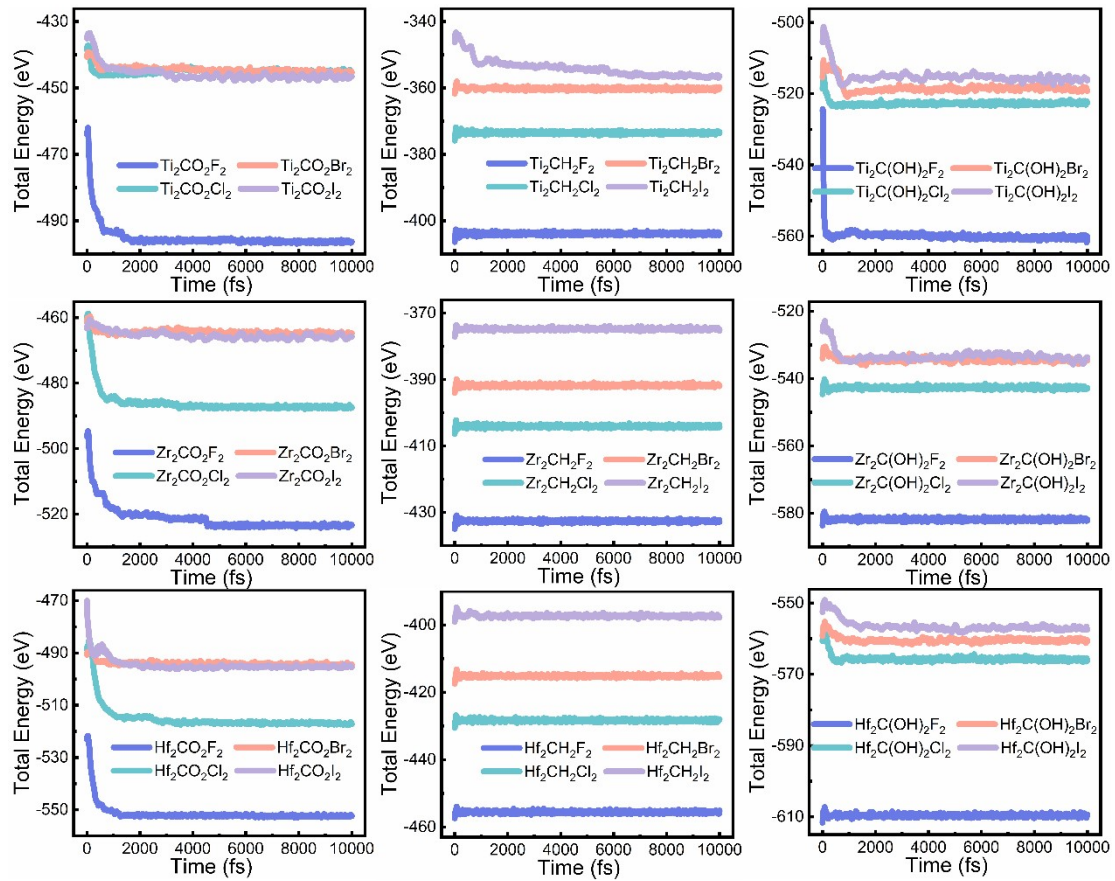
Fig. S11 Variation curves in total energy for all monolayer adsorption models at the conditions of 300 K, 10 ps, and NVT ensemble.

11
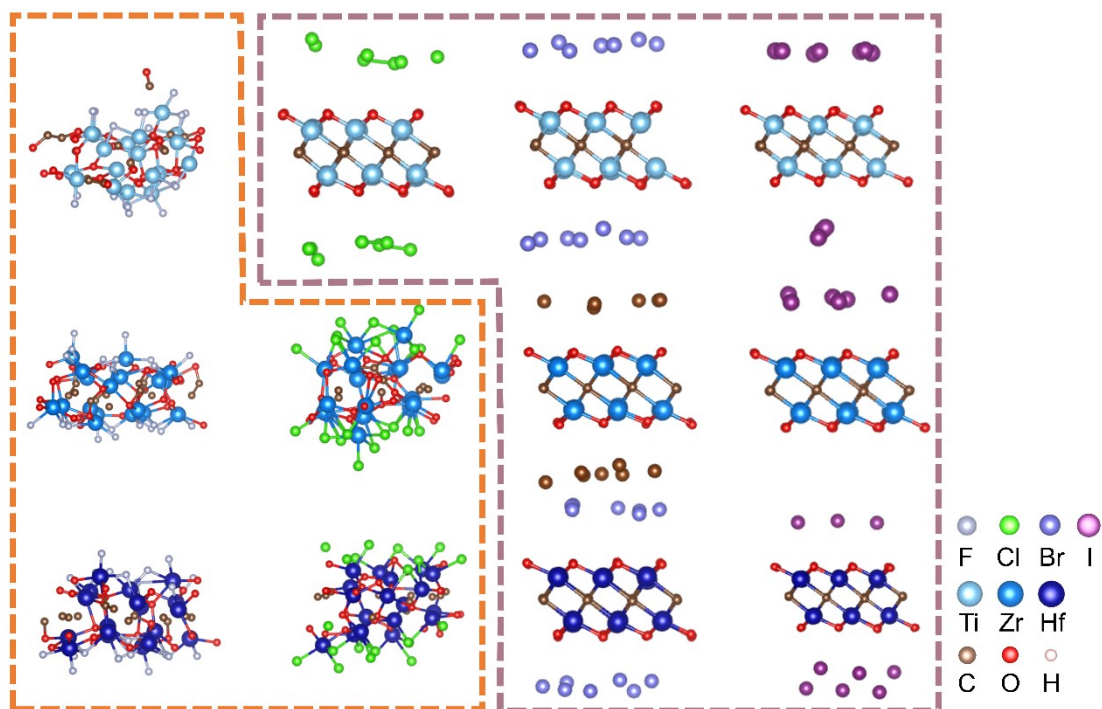
Fig. S12 Configurations of monolayer adsorption models on O-functionalized MXenes after AIMD simulations at the conditions of 300 K, 10 ps, and NVT ensemble. Orange area represents "Broken" and brown area represent "Desorption".
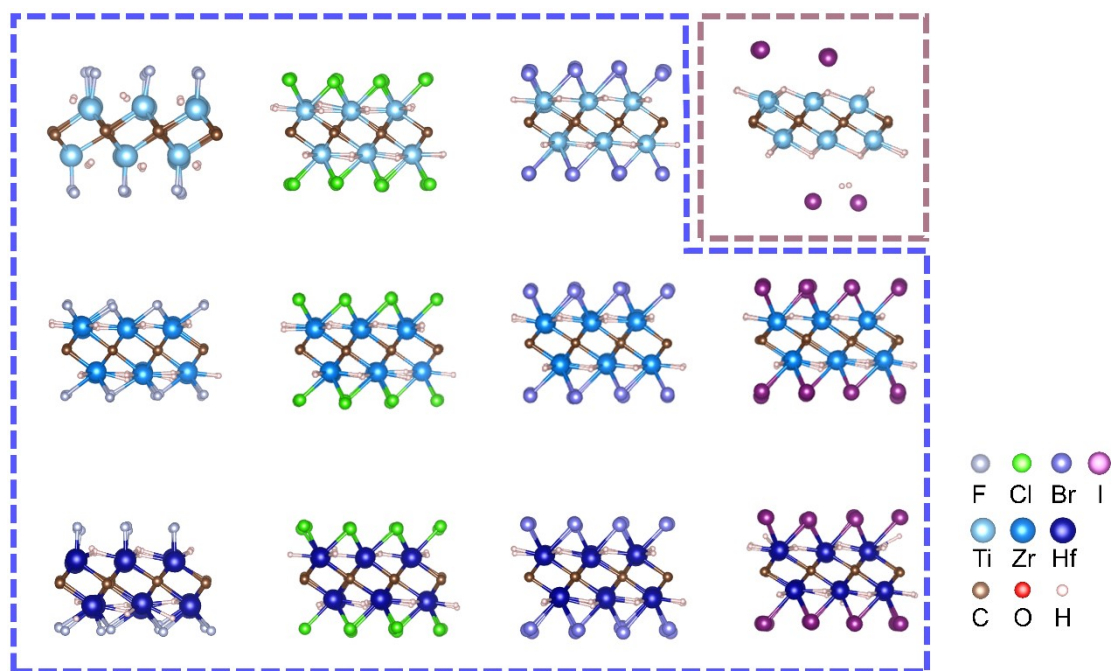
Fig. S13 Configurations of monolayer adsorption models on H-functionalized MXenes after AIMD simulations at the conditions of 300 K, 10 ps, and NVT ensemble. Blue area represents "Stable" and brown area represent "Desorption".
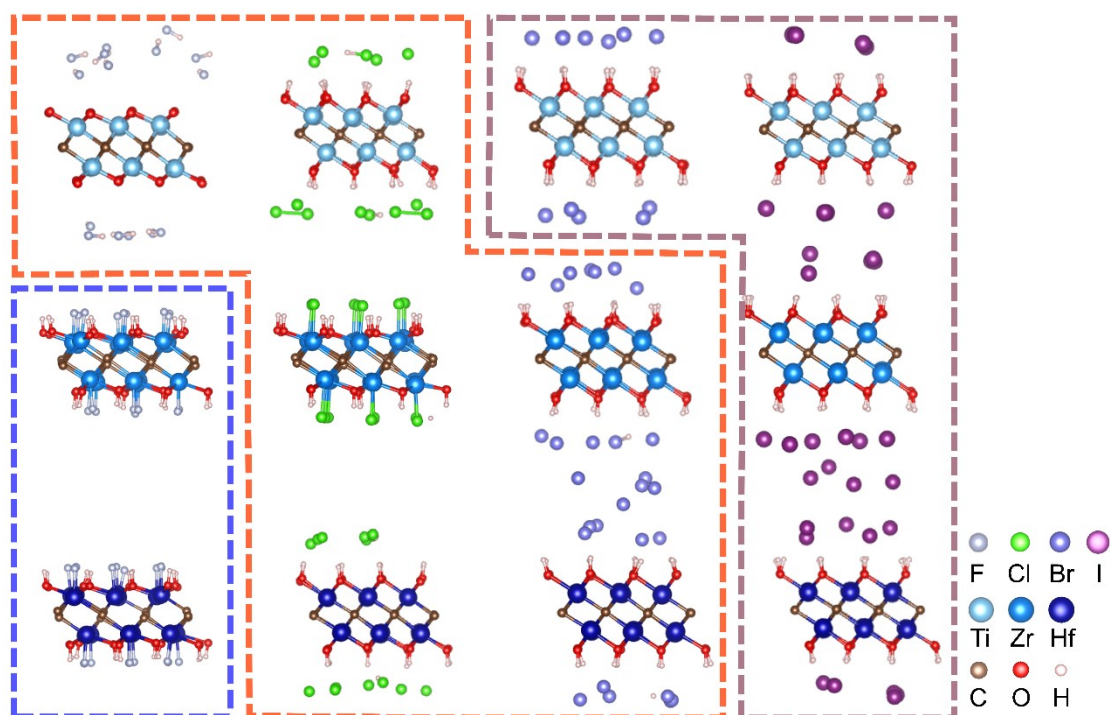
Fig. S14 Configurations of monolayer adsorption models on OH-functionalized MXenes after AIMD simulations at the conditions of 300 K, 10 ps, and NVT ensemble. Blue area represents "Stable"; Orange area represents "Broken" and brown area represent "Desorption".
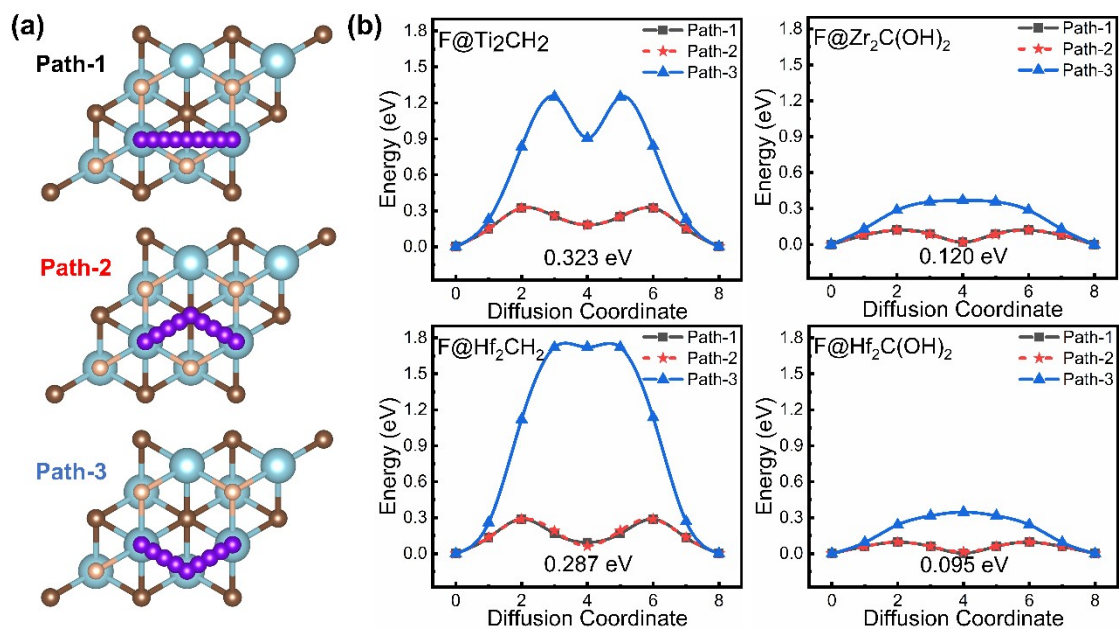
Fig. S15 The diffusion paths for halogen ions stably adsorbed on the T_M site (a). The corresponding diffusion energy barriers of halogen ions on MXenes (b).
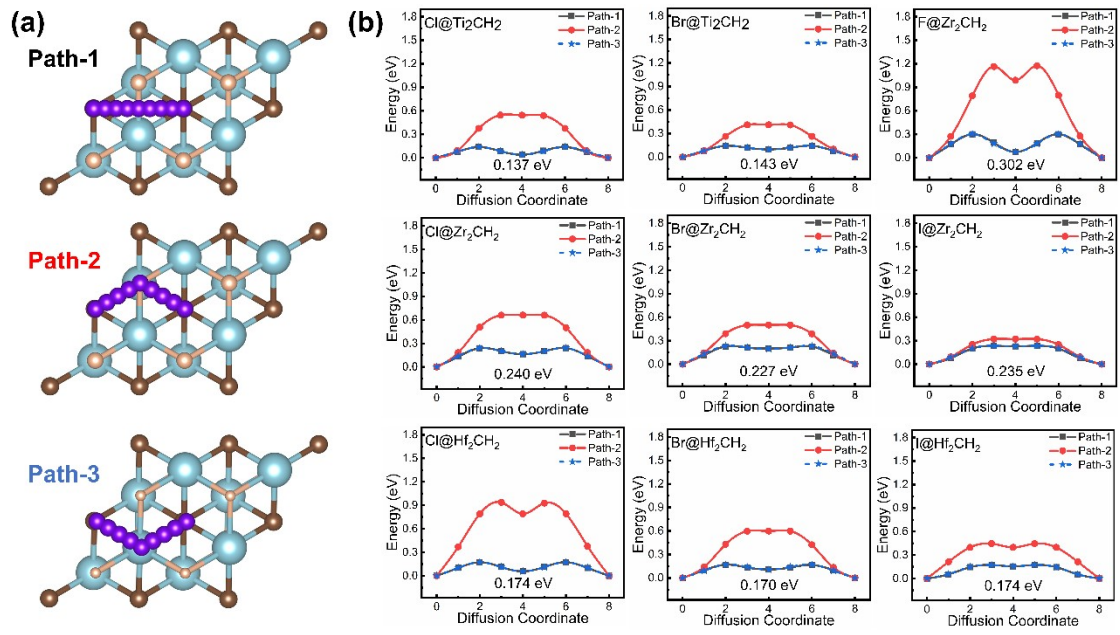
Fig. S16 The diffusion paths for halogen ions stably adsorbed on the T_c site (a). The corresponding diffusion energy barriers of halogen ions on MXenes (b).
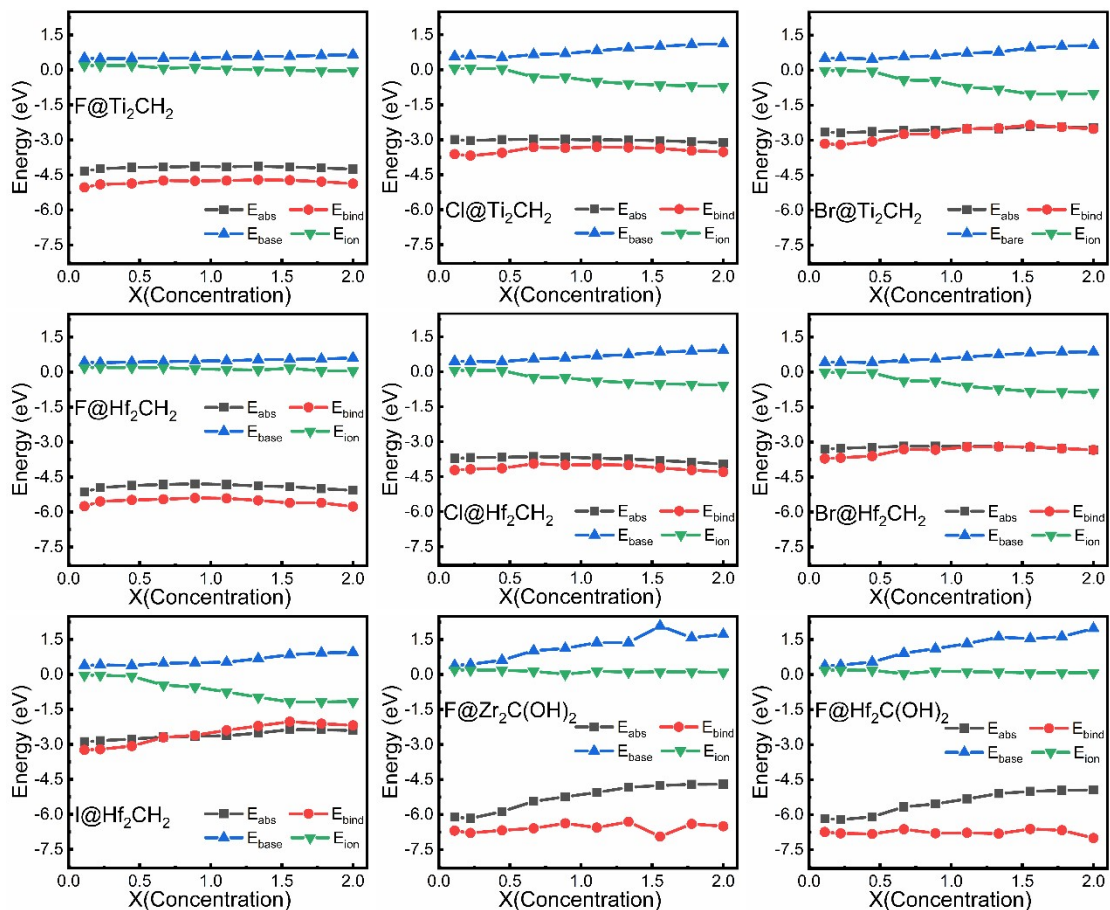
Fig. S17 Energy variation curves with the concentration of inserted ions for halogen ions adsorbed on MXenes.

Table S1 Optimized structure parameters and formation energy of all M_2CH_2 MXene models.

System	Model	Parameter α(Å)	Thickness d(Å)	Bond length(Å) Nearest			Formation energy (eV)
				M-C	M-M	M-H	
	I	3.168	5.681	2.130	2.850	1.747	0.676
Ti_2CH_2	II	3.010	4.275	2.088	2.894	1.995	-2.876
	III	2.942	4.665	2.084	2.953	2.037	-2.191
	I	3.400	6.236	2.313	3.129	1.900	0.849
Zr_2CH_2	II	3.287	4.550	2.275	3.145	2.155	-2.954
	III	3.207	5.934	2.269	3.212	2.198	-2.376
	I	3.306	6.368	2.286	3.154	1.879	0.673
Hf_2CH_2	II	3.233	4.526	2.239	3.098	2.130	-3.013
	III	3.171	4.934	2.239	3.160	2.178	-2.408

Table S2 Optimized structure parameters of M_2CT_2 MXenes.

Model	Parameter α(Å)	Thickness d(Å)	Bond length(Å) Nearest		
			M-C	M-M	M-T
Ti_2CO_2	3.015	4.440	2.175	3.015	1.968
Ti_2CH_2	3.010	4.275	2.088	2.894	1.995
$Ti_2C(OH)_2$	3.038	6.794	2.100	3.038	2.164
Zr_2CO_2	3.295	4.639	2.359	3.295	2.115
Zr_2CH_2	3.287	4.550	2.275	3.145	2.155
$Zr_2C(OH)_2$	3.294	7.394	2.267	2.295	2.340
Hf_2CO_2	3.252	4.611	2.327	3.252	2.097
Hf_2CH_2	3.233	4.526	2.239	3.098	2.130
$Hf_2C(OH)_2$	3.257	7.058	2.236	3.257	2.310

Table S3 Comparison of electrochemical performance between this work and previous reports.

Systems	Type [a]	Capacity (mAh/g)	Max Working Voltage (V) [b]	Voltage Change (V) [c]	Diffusion energy barrier (eV)	Experiment or Calculation	Reference
BiF_3	F	126	2.61 vs Ce	-1.61	\	Exp.	Ref. 1
$LaSrMnO_4$	F	100	2.00 vs PbF_2	-2.00	\	Exp.	Ref. 2
La_2CoO_4	F	30	1.00 vs PbF_2	-2.00	\	Exp.	Ref. 3
CuF_2	F	360	3.00 vs La	-2.00	\	Exp.	Ref. 4
Ca_2N	F	285	2.31 vs PbF_2	\	0.20	Cal.	Ref. 5
Y_2CF_2	F	282	2.01 vs PbF_2	\	0.16	Cal.	Ref. 5
Sr_2NF	F	141	2.21 vs PbF_2	\	\	Cal.	Ref. 5
Ba_2LiNF_2	F	181	2.05 vs PbF_2	\		Cal.	Ref. 5
$Sr_2TiO_3F_2$	F	198	2.01 vs PbF_2	\	\	Cal.	Ref. 5
Sr_2FeO_3F	F	96	0.78 vs PbF_2	\	\	Cal.	Ref. 5
Ti_2CH_2	**F**	**488**	**4.43 vs Li**	**-0.08**	**0.32**	**Cal.**	**This Work**
Zr_2CH_2	**F**	**273**	**5.30 vs Li**	**+0.32**	**0.30**	**Cal.**	**This Work**
Hf_2CH_2	**F**	**144**	**5.23 vs Li**	**-0.07**	**0.29**	**Cal.**	**This Work**
$Zr_2C(OH)_2$	**F**	**234**	**6.21 vs Li**	**-1.23**	**0.12**	**Cal.**	**This Work**
$Hf_2C(OH)_2$	**F**	**133**	**6.27 vs Li**	**-1.26**	**0.10**	**Cal.**	**This Work**
FeOCl	Cl	20	2.50 vs Mg	-1.80	\	Exp.	Ref. 6
VOCl	Cl	113	2.80 vs Li	-1.80	\	Exp.	Ref. 7
CoFe-LDH	Cl	160	3.00 vs Li	-1.80	0.15	Exp. & Cal.	Ref. 8
CoOCl	Cl	243	3.50 vs LiCl	-1.30	0.37	Cal.	Ref. 9
FeOCl	Cl	250	2.60 vs LiCl	-1.20	0.58	Cal.	Ref. 9
VOCl	Cl	262	3.60 vs LiCl	-1.50	0.65	Cal.	Ref. 9
Ti_2C	Cl	331	4.00 vs Li	-0.50	0.22	Cal	Ref. 10
$Ti_2C(OH)_2$	Cl	126	3.50 vs Li	-2.00	0.06	Cal	Ref. 10
Ti_2CH_2	**Cl**	**488**	**3.13 vs Li**	**+0.13**	**0.14**	**Cal.**	**This Work**
Zr_2CH_2	**Cl**	**273**	**4.61 vs Li**	**+0.32**	**0.24**	**Cal.**	**This Work**
Hf_2CH_2	**Cl**	**144**	**4.61 vs Li**	**+0.39**	**0.17**	**Cal.**	**This Work**
MoS_2	Br	151	1.78 vs Zn	-0.78	\	Exp.	Ref. 11
Carbon Black	Br	175	1.82 vs Zn	-1.40	\	Exp.	Ref. 12
$BiBr_3$	Br	157	0.60 vs $PbBr_2$	-0.60	\	Exp.	Ref. 13
Ti_2CH_2	**Br**	**488**	**2.66 vs Li**	**-0.19**	**0.14**	**Cal.**	**This Work**
Zr_2CH_2	**Br**	**273**	**2.55 vs Li**	**+0.20**	**0.28**	**Cal.**	**This Work**
Hf_2CH_2	**Br**	**144**	**3.50 vs Li**	**+0.02**	**0.17**	**Cal.**	**This Work**
Carbon Black	I	83	1.23 vs Zn	-0.83	\	Exp.	Ref. 14
Zr_2CH_2	**I**	**488**	**2.65 vs Li**	**-0.23**	**0.24**	**Cal.**	**This Work**
Hf_2CH_2	**I**	**273**	**2.76 vs Li**	**-0.48**	**0.17**	**Cal.**	**This Work**

[a] Only ion intercalation batteries are considered

[b] + sign indicates an increase in voltage relative to the initial voltage, - sign indicates a decrease.

Table S4 Contribution of each energy composition for adsorption energy for halogen ions adsorbed on Zr_2CH_2 MXene.

Type	F Absolute (eV)	Relative (%)	Cl Absolute (eV)	Relative (%)	Br Absolute (eV)	Relative (%)	I Absolute (eV)	Relative (%)
Binding Energy	-0.691	213.8	-0.221	56.8	0.233	-115.2	0.920	394.1
Bare Energy	0.549	-169.9	0.445	114.5	0.376	-185.9	0.427	182.8
Ion Energy	-0.181	56.1	-0.613	157.7	-0.810	401.2	-1.113	-476.9
Total	-0.323	100.0	-0.389	100.0	-0.202	100.0	0.233	100.0

Supplementary Discussion 1

To explain the formation of nearly free electron gas (NFE) at the vacuum layer on H- and OH-functionalized MXenes, we conducted the calculation of the differential charge density and electrostatic potential. Here, we take Hf_2CT_2 MXenes as examples, the corresponding differential charge density results are shown in Figure S8(a-c). The results show that charges will accumulate around the C atoms for all functionalized MXenes. And the O atoms in the O- and OH-functionalized MXenes accumulate more charges. Besides, no charge accumulation was found at the vacuum layer on the Hf_2CH_2 surface, which may be ascribed to the low content of the nearly free electrons. Significant charge accumulation was found at the vacuum layer on $Hf_2C(OH)_2$, which is consistent with the ELF results. Compared with Hf_2CO_2, the NFE states of $Hf_2C(OH)_2$ originate from the positive charge on the surface. Margine et al. studied the effect of positive surface charge on NFE states. [15] The results show that the NFE states are mainly concentrated near the maximum positive charge, and the NFE states will be closer to the Fermi level as the surface positive charge increases. Lu et al. proposed that surface dipoles also have a significant effect on NFE states.[16]

Since the NFE states can be only formed in the spatial regions away beyond the surfaces toward the vacuum in the electrostatic potential wells. [17] Therefore, the electrostatic potential can be better used to analyze the formation of NFE states. The calculated total average potentials of Hf_2CO_2, Hf_2CH_2 and $Hf_2C(OH)_2$ are shown in Figure S8(d-f). Since NFE states only occur in the vacuum region away from the surface, the tail shape of the electrostatic potential determines where the NFE states locate. It can be seen that the potential tail of $Hf_2C(OH)_2$ is shallower and more extended, while that of Hf_2CO_2 is the deepest and narrowest. This means that the NFE electronic states of $Hf_2C(OH)_2$ will be found near the Fermi level, which is intuitively observed in the ELF diagram. Nevertheless, the NFE states of Hf_2CO_2 will be transferred to higher energies that cannot observed in the ELF diagram. The results of the differential charge density and the electrostatic potential of Ti_2CT_2 and Zr_2CT_2 MXenes can be found in Figure S6 and Figure S7, and similar conclusions can also be obtained.

The work function is the difference between the Fermi level and the vacuum level, which can effectively represent the shape and distribution of electrostatic potential. Here, we establish the function between the work function and the net charge of the surface atoms in Figure S10. We can

22

find that the OH-functionalized MXenes have the lowest work function and the highest amount of positive charge. So, the positive surface charge H leads to a lower work function, which in turn generates a large number of NFE states at Fermi Level. And the slightly negatively charged H-terminal may have few numbers of NFE states in ELF diagram while no NFE states can be observed on O-functionalized MXenes. Hence, the positive surface charge makes a significant effect on the location of NFE states, and the NFE states will be closer to the Fermi level as the surface positive charge increases. Besides, it should be emphasized that the work function and surface charge can only determine the occurrence position of NFE states and cannot quantify the content of NFE states.

References

1. M. Anji Reddy and M. Fichtner, *J. Mater. Chem.*, 2011, **21**, 17059-17062.
2. M. A. Nowroozi, K. Wissel, J. Rohrer, A. R. Munnangi and O. Clemens, *Chem. Mater.*, 2017, **29**, 3441-3453.
3. M. A. Nowroozi, S. Ivlev, J. Rohrer and O. Clemens, *J. Mater. Chem. A*, 2018, **6**, 4658-4669.
4. D. T. Thieu, M. H. Fawey, H. Bhatia, T. Diemant, V. S. K. Chakravadhanula, R. J. Behm, C. Kübel and M. Fichtner, *Adv. Funct. Mater.*, 2017, **27**, 1701051.
5. S. T. Hartman and R. Mishra, *J. Mater. Chem. A*, 2020, **8**, 24469-24476.
6. X. Zhao, Q. Li, Z. Zhao, Karger, P. Gao, K. Fink, X. Shen and M. Fichtner, *ACS Appl. Mater. Interfaces*, 2014, **6**, 10997-11000.
7. P. Gao, M. A. Reddy, X. Mu, T. Diemant, L. Zhang, Z. Zhao-Karger, V. S. K. Chakravadhanula, O. Clemens, R. J. Behm and M. Fichtner, *Angew. Chem. Int. Ed.*, 2016, **55**, 4285-4290.
8. Q. Yin, D. Rao, G. Zhang, Y. Zhao, J. Han, K. Lin, L. Zheng, J. Zhang, J. Zhou and M. Wei, *Adv. Funct. Mater.*, 2019, **29**, 1900983.
9. M. Wu, X. Lv, J. Wang, R. Wang, X. Shi, H. Zhang, C. Jin, Y. Wei and R. Lian, *J. Mater. Chem. A*, 2021, **9**, 23169-23177.
10. D. Wang, Y. Gao, Y. Liu, Y. Gogotsi, X. Meng, G. Chen and Y. Wei, *J. Mater. Chem. A*, 2017, **5**, 24720-24727.
11. H. Zhao, M. Li, Z. Fang and Q. Su, *Inorg. Chem. Commun.*, 2021, **133**, 108873.
12. H. Li, M. Li, X. Zhou, T. Li and H. Zhao, *Sustain. Energ. Fuels*, 2020, **4**, 3871-3878.
13. A. Inoishi, M. Hokazono, E. Kashiwazaki, N. Setoguchi, T. Sakai, R. Sakamoto and S. Okada, *ChemElectroChem*, 2021, **8**, 246-249.
14. H. Li, M. Li, X. Zhou and T. Li, *J. Power Sources*, 2020, **449**, 227511.
15. E. R. Margine and V. H. Crespi, *Phys. Rev. Lett.*, 2006, **96**, 196803.
16. N. Lu, Z. Li and J. Yang, *J. Phys. Chem. C*, 2009, **113**, 16741-16746.
17. M. Khazaei, A. Ranjbar, M. Ghorbani-Asl, M. Arai, T. Sasaki, Y. Liang and S. Yunoki, *Phys. Rev. B*, 2016, **93**, 205125.